Chemical Engineering Science 110 (2014) 31–43

Contents lists available at ScienceDirect

Chemical Engineering Science

journal homepage: www.elsevier.com/locate/ces

Simulation of the coking phenomenon in the superheater of a steam cracker

Amit V. Mahulkar, Geraldine J. Heynderickx *, Guy B. Marin

Laboratory for Chemical Technology, Ghent University, Technologiepark 914, B-9052 Gent, Belgium

HIGHLIGHTS

- Coke formation in convection section of steam cracker is simulated using CFD.
- Coking occur due to thermal degradation of liquid feed deposited on tube wall.
- Thickest coke layer is observed in inlet-bend due to impingement of droplets.
- Complete evaporation of the heavy feed would eliminate the coke formation.
- Feed spray with finer droplet size would reduce the coking rates.

ARTICLE INFO

Article history:
Received 3 May 2013
Received in revised form
8 July 2013
Accepted 8 August 2013
Available online 22 August 2013

Keywords:
Coke formation
Steam cracking
CFD
Convection section
Spray flow

ABSTRACT

Coke formation in the convection section of a steam cracker occurs when heavy feeds are cracked. This work presents CFD simulations of coke formation in the mixture superheater tubes in the convection section of a steam cracker. The hydrocarbon feed used for the simulations is a gas condensate. Eleven representative chemical species are selected, based on their boiling points, to mimic the entire range of feed components. The liquid–vapor spray flow in the mixture superheater tube is simulated based on an Eulerian–Lagrangian approach using ANSYS FLUENT 13.0. Evaporation of multicomponent droplets suspended in the vapor phase or deposited on a tube wall is considered. The mixture superheater tubes make three horizontal passes (11.3 m long and 0.077 m diameter) through the convection section. The droplet–wall interaction model considers 'Splash', 'Rebound induced breakup', 'Rebound' and 'Stick'. The amount of liquid deposited on the mixture superheater tube wall is obtained by simulating the spray flow. The amount of coke formed from the liquid deposited on a wall is based on the phase separation model of (Wiehe, 1993). Industrial & Engineering Chemistry Research 32, 2447–2454. Spatial variations of the coke layer formed in the mixture superheater tubes as a function of outer tube wall temperatures and initial droplet diameter are presented. For outer tube wall temperatures lower than the boiling point of the highest-boiling species in the feed a 1 mm thick coke layer is formed over a period of 1 month. For outer tube wall temperatures higher than the boiling point of the highest boiling component in the feed no coke is formed in the mixture superheater tubes. This work provides guidelines to minimize the extent of coke formation in the steam cracker convection section when a heavy feed is cracked. It also provides possible remedies to completely eliminate the coking problem when cracking heavy feeds.

1. Introduction

Due to an ever increasing demand to produce lighter and more valuable hydrocarbons like ethylene and propylene on the one hand, and an increasing supply of cheaper but heavier crude oil on the other hand, the industrial steam crackers are forced to operate with heavy feeds. It is very likely that the operating protocol and/or the design of the existing industrial steam crackers will need to be adapted. It can be expected that these changes will essentially involve increasing the heat input in the steam cracker in order to retain complete evaporation and sufficient over-heating of the heavier crude oil feeds within the convection section of the steam cracker. In this work, with the help of CFD simulations, the magnitude of possible fouling problem due to the use of heavy feeds is estimated and the remedies to avoid the same are suggested. The constructional features of the convection section of steam cracker are taken from the earlier work of De Schepper et al. (2010). In the convection section three types of heat exchangers are placed one below the other (Fig. 1(a)). In the top, where flue gas temperatures are low, a liquid feed evaporator is

* Corresponding author. Tel.: +32 9 264 45 32; fax: +32 9 264 45 99.
E-mail address: Geraldine.Heynderickx@UGent.be (G.J. Heynderickx).

0009-2509/$ - see front matter © 2013 Elsevier Ltd. All rights reserved.
http://dx.doi.org/10.1016/j.ces.2013.08.021

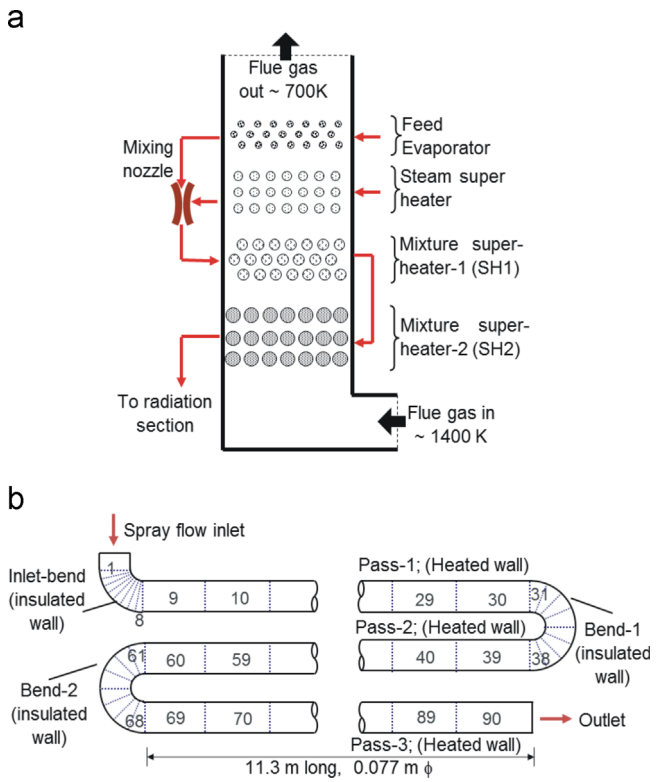

Fig. 1. (a) Schematic view of convection section and (b) superheater tube geometry with boundary conditions.

placed. Below the feed evaporator a steam superheater is positioned and in the bottom of the convection section, where flue gas temperatures are high, two feed-steam mixture superheaters (SH1 and SH2) are placed. The partially evaporated feed leaving the feed evaporator is mixed with the over-heated steam in a mixing nozzle, where the remaining liquid fraction of the feed is supposed to be completely evaporated. However, the use of heavier feeds requires more energy for the evaporation. If the enthalpy of the steam is not sufficient to completely evaporate the feed, the residual liquid atomizes into a spray flow in the nozzle. This spray flow enters the mixture superheater where some fraction of the droplets will be deposited on the inner tube walls. The deposited liquid undergoes thermal degradation, resulting into coke formation on the inner tube walls. The coke formation increases the number of shut-downs due to the required decoking of the convection section in addition to the decoking shut-downs required for the radiation section tubes. The ideal solution to overcome this problem is to ensure a complete evaporation of the feed before it enters the mixture superheater tubes. However, this is not straightforward as the convection section uses the heat remaining in the flue gas coming from the radiation section of the steam cracker. Since the temperature in the radiation section is a critical parameter, as it determines the feed conversion and product yields, it also determines the flue gas temperature entering the convection section. This limits the energy available in the convection section for evaporation and over-heating purpose and, hence, the demand for extra heat to ensure a complete evaporation of a heavy feed cannot be met without external heat supply. Furthermore, the extra heat supply can be limited by the maximum allowable temperature of the tube wall material in the convection section.

In the past, efforts were taken to improve the design of the mixing nozzle that would either minimize the spray formation or avoid the spray droplets from impinging on the mixing nozzle wall (Chandrasekharan et al., 2005; Grondman, 1983). Such nozzles reduce the spray formation but will not completely eliminate the spray formation. Thus the spray flow formation and liquid deposition on the wall are not avoided. Hence, the behavior of spray flow in the mixture superheater tubes has to be studied. In the present study, spray flow and subsequent coke formation in the mixture superheater tubes in the convection section of a steam cracker is simulated. The coke formation is studied as a function of different operating conditions like the temperature of the flue gas flowing through the convection section, the initial droplet diameter and the geometry of the mixture superheater tubes. Spray flow and coke formation in the mixture superheater tubes of the convection section was previously studied and reported by De Schepper et al. (2010), in a first attempt to simulate the complex phenomena of droplet flow, impingement of droplet on tube walls and subsequent coke formation in the convection section of a steam cracker. This study was based on a number of simplifying assumptions. E.g. the feed was a 'simulated' feed with some very heavy chemical species. The boiling point of the droplets was assumed to be constant (511 K), irrespective of the composition of the droplet. The droplet splashing was limited to only three splashed droplets (daughter droplets) being formed independent of the Weber number of the impinging droplet. In present work the coke formation model used is more relevant to the condition in convection section of steam cracker. The present work improves the applied models and provides more refined results for the coking problem in the convection section tubes of a steam cracker. The effect of these refinements over the previous model will be highlighted in the manuscript at appropriate places.

2. Problem description

The geometry of the mixture superheater tubes in the convection section of an operating industrial steam cracker has already been extensively reported by De Schepper et al. (2010). The same geometry of mixture superheater tubes is used in the present study (Fig. 1). There are two mixture superheaters, referred to as superheater-1 (SH1) and superheater-2 (SH2), in the convection section. The two superheaters are placed sequentially one after the other for stepwise over-heating of the feed-steam mixture. Coke formation is possible in both superheaters (SH1 and SH2), but coking will be first observed in SH1. Thus in the present work coke formation in SH1 is studied. The SH1 tubes are 11.3 m long, have a diameter of 0.077 m, a wall thickness of 0.005 m and make three horizontal passes through the convection section (Fig. 1). The feed-steam mixture enters the 90° 'Inlet-bend' connecting the mixing nozzle with the first horizontal tube pass, referred to as 'Pass-1'. The remaining two horizontal passes, named 'Pass-2' and 'Pass-3' are connected by two U-bends, referred to as 'Bend-1' and 'Bend-2' (Fig. 1). The U-bends are insulated and are located outside the convection section. Thus in the simulations the bends are treated as adiabatic walls. The hot flue gas, coming from the radiation section of the steam cracker, flows over the tubes. The tubes are simulated as heated walls with a uniform outer wall temperature. Thermal resistances of the metallic tube wall, of the coke layer (wherever formed) and of the internal fluid film resistance are accounted for in the simulations.

About 30 wt% of the liquid hydrocarbon feed remains unevaporated at the exit of the evaporator (De Schepper et al., 2010). The partially evaporated feed is then mixed with the over-heated steam in a feed-steam mixing nozzle. In the mixing nozzle the feed undergoes further evaporation. Based on overall mass and energy balances over the mixing nozzle, where the over-heated steam (5 bar, 600 K, 0.55 kg/s) is mixed with the partially vaporized feed (30 wt% liquid and 70 wt% vapor, 0.55 kg/s), it is seen that the liquid fraction of the feed further reduces to 14 wt%.

The remaining liquid feed fraction is atomized into a spray of fine droplets upon mixing with the over-heated steam. The total inlet (hydrocarbon vapor, hydrocarbon droplets and steam) mass flow rate for one SH1 tube is 1.1 kg/s with a hydrocarbon feed to steam ratio of 0.5 (wt%). Thus, the droplet flow rate at the inlet of a mixture superheater tube is 0.077 kg/s. In the present study, the coking rate and the coke layer position in the tubes are determined for three different SH1 outer tube wall temperatures (650, 700 and 750 K) and four different initial droplet diameters (100, 50, 10 and 1 μm). The outer wall temperature is chosen such that its value is less than, equal to and above the boiling point of the highest boiling species in the gas condensate feed. The three tube passes and the tube bends are divided in small sections and numbered (Fig. 1) to facilitate the presentation and discussion of the simulation results.

3. Numerical models

3.1. Spray flow model

Computational fluid dynamics (CFD) simulations are performed using ANSYS FLUENT 13.0 which uses the finite volume (FV) approach to solve the set of conservation equations. To simulate the spray flow an Eulerian–Lagrangian approach is used. The Reynolds-Averaged Navier–Stokes (RANS) equations are solved to determine the velocity field of the continuous phase. Since the flow in the mixture superheater tubes is turbulent ($Re > 100{,}000$) the Reynolds stresses originating from the turbulence contribution in the RANS equations needs to be closed with an appropriate turbulence model. In present study, the continuous phase flow is unidirectional pipe flow with no swirling motion and near isotropic turbulence. Hence the standard k–ε turbulence model suffices to simulate turbulence in the continuous phase (Launder and Spalding, 1974). Since the tube wall is heated and the liquid droplet, in the vapor phase or deposited on wall, undergoes evaporation, it is essential to simulate the energy balance for both the continuous and the discrete phase. The wall heat transfer coefficient is based on standard wall functions available in FLUENT 13.0. The standard wall functions are also used to determine the velocity and the turbulence near the wall. The conservation and the turbulence equations used in the present study are shown in Table 1.

A gas chromatographic analysis of a gas condensate feed shows that it is composed of about 120 chemical species. These chemical species are found to have a very wide boiling point range (300–750 K). Hence, the physical properties of the gas condensate feed, like vapor pressure and boiling point, vary significantly as the evaporation proceeds. In order to be able to take this variation in physical properties into account during the simulations, 11 representative species are selected from the feed. These 11 species are selected such that they represent the entire feed of 120 chemical species in terms of the boiling point variation from the lightest to the highest boiling chemical species in the gas condensate feed. The simulations are performed using these representative feed species. The boiling point curve of the actual feed is shown in Fig. 2 with the representative species marked on it. The x-axis of Fig. 2 shows, the cumulative weight fraction of the species, from the 'low boilers' (species with lower boiling temperatures) to the 'high boilers' (species with higher boiling temperatures). In the present study, the species continuity equation for each of the 11 representative species is solved (Table 1). The physical properties for the selected species are shown in Table 2.

ANSYS FLUENT 13.0 uses the Lagrangian approach to simulate a discrete phase flow. The velocity of an individual droplet is obtained by integrating the force balance over the droplet (see Eq. (h), Table 3) (ANSYS, 2010). The location of the droplet is obtained from the velocity of droplet using Eq. (i) in Table 3. As the droplet flows through the SH1 tubes, it will add mass to the continuous phase due to evaporation of species from the droplet, exchange momentum due to drag between the droplet and the continuous phase, and exchange thermal energy due to

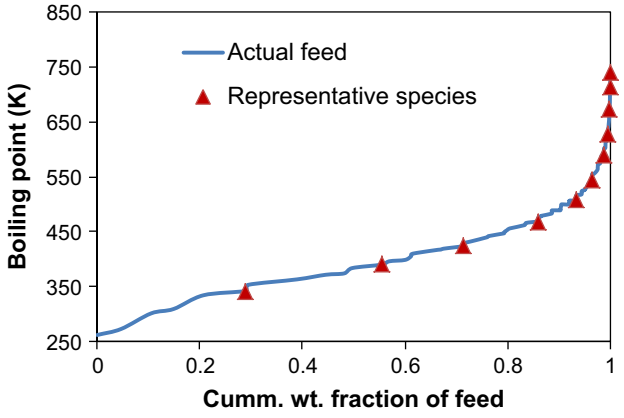

Fig. 2. Boiling point curve for the feed. Selected representative species.

Table 1
Mass, momentum and energy equations for continuous (vapor) phase.

Mass balance

$$\frac{\partial}{\partial t}(\rho)+\nabla\cdot(\rho\vec{u})=\sum_{j}S_{Mj} \quad (a)$$

Species mass balance

$$\frac{\partial}{\partial t}(\rho Y_j)+\nabla\cdot(\rho\vec{u}Y_j)=-\nabla\cdot\left[\left(\rho D_{j,m}+\frac{\mu_t}{0.7}\right)\nabla Y_j\right]+S_{M,j} \quad (b)$$

Momentum balance

$$\frac{\partial}{\partial t}(\rho\overline{u}_i)+\nabla\cdot(\rho\vec{u}\vec{u})=-\nabla P+\nabla\cdot\left[\mu\left(\nabla\vec{u}+\nabla\vec{u}^{T}-\frac{2}{3}\nabla\cdot\vec{u}I\right)\right]+\nabla\cdot(\rho\vec{u'}\vec{u'})+\rho g_i+S_{F,i} \quad (c)$$

Energy balance

$$\frac{\partial}{\partial t}(\rho E)+\nabla\cdot(\rho\vec{u}E)=\nabla\cdot[(K+K_t)\nabla T-\sum_{j}C_{p,j}T\vec{J}_j]+S_E \quad (d)$$

$$E=\sum_{j}Y_j\left(\int_{T_{ref}}^{T}C_{P,j}dT\right)+\frac{P}{\rho} \quad (e)$$

Turbulence model

Turbulent kinetic energy balance

$$\frac{\partial}{\partial t}(\rho k)+\nabla\cdot(\rho k\vec{u})=\nabla\cdot\left[\left(\mu+0.09\rho\frac{k^2}{\varepsilon}\right)\nabla k\right]+G_k+G_b-\rho\varepsilon \quad (f)$$

Turbulent energy dissipation rate balance

$$\frac{\partial}{\partial t}(\rho\varepsilon)+\nabla\cdot(\rho\varepsilon\vec{u})=\nabla\cdot\left[\left(\mu+\frac{\mu_t}{1.3}\right)\nabla\varepsilon\right]+1.44\frac{\varepsilon}{k}(G_k+C3G_b)-1.92\rho\frac{\varepsilon^2}{k} \quad (g)$$

Table 2
Feed properties and composition of vapor and droplets at mixer superheater tube inlet.

S. no.	Species	Boiling point (K)	wt%	Antoine equation* parameters (bar, K)			Latent heat (kJ/kg)	Composition (%)	
				A	B	C		Droplet	Vapor
1	Species-a	342.0	28.90	4.00266	1171.5	−48.78	335.0	0.0	16.8
2	Species-b	391.5	26.57	4.04227	1337.4	−59.45	291.7	0.0	15.45
3	Species-c	424.0	15.98	4.06245	1430.3	−71.35	287.7	0.0	9.29
4	Species-d	469.0	14.48	4.10164	1572.4	−85.12	265.5	0.0	8.41
5	Species-e	507.0	7.37	4.12829	1689.0	−98.86	247.5	52.14	0.040
6	Species-f	542.0	3.12	4.14935	1789.6	−111.85	232.8	22.28	0.0
7	Species-g	590.0	2.33	4.33209	2068.9	−111.92	214.0	16.64	0.0
8	Species-h	629.5	0.78	4.20190	2022.5	−147.5	198.2	5.57	0.0
9	Species-I	674.9	0.35	4.22870	2138.8	−168.4	180.9	2.5	0.0
10	Species-j	713.8	0.09	4.25050	2233.6	−187.6	166.3	0.64	0.0
11	Species-k	740.5	0.03	4.26490	2296.1	−201.4	156.8	0.21	0.0
12	Water	373.0	–	–	–	–	–	–	50.0

* Antoine equation $\log_{10}(P)=A-(B/(T+C))$. Vapor pressure (P) in bar and temperature (T) in K.

Table 3
Discrete phase model equations and source terms for continuous phase.

Force balance over the particle

$$\frac{du_{d,i}}{dt}=\frac{18\mu}{\rho_d d_d^2}\times\frac{C_D}{24}\times\frac{\rho\, d_d|u_i-u_{d,i}|}{\mu}\times(u_i-u_{d,i})+\frac{g_i(\rho_d-\rho)}{\rho_d} \quad \text{(h)}$$

Particle positioning

$$\frac{dx_{d,i}}{dt}=u_{d,i} \quad \text{(i)}$$

Momentum source term for the continuous phase due to the presence of the dispersed phase

$$S_{F,i}=\sum_0^{t_c}\left[\left[\frac{18\mu}{\rho_d d_d^2}\times\frac{C_D}{24}\times\frac{\rho\, d_d|u_i-u_{d,i}|}{\mu}\times(u_i-u_{d,i})\right]\frac{m_d}{m_{d,0}}\dot{m}_{d,0}\times\Delta t\right] \quad \text{(j)}$$

Energy source term for the continuous phase due to the presence of the dispersed phase

$$S_E=\frac{m_{d,in}}{m_{d,0}}\dot{m}_{d,0}\sum_j Y_j\left(\int_{T_{ref}}^{T_{d,in}}C_{P,j}dT\right)-\frac{m_{d,out}}{m_{d,0}}\dot{m}_{d,0}\sum_j Y_j\left(\int_{T_{ref}}^{T_{d,out}}C_{P,j}dT\right)-\frac{\Delta m_d}{m_{d,0}}\dot{m}_{d,0}\sum_j Y_j h_{fg,j} \quad \text{(k)}$$

Mass source term for the continuous phase due to the presence of the dispersed phase

$$S_M=\frac{\Delta m_d}{m_{d,0}}\dot{m}_{d,0} \quad \text{(l)}$$

$$\Delta m_d=\sum_j\left[k_c\left(\frac{x_j P_{sat}(T_d)}{RT_d}-\frac{Y_j P)}{RT_\infty}\right)\times 4\pi d_d^2\times t_c\right] \quad \text{(m)}$$

evaporation and heat exchange with the continuous phase. These exchange terms are added as discrete phase source terms in the mass, momentum and energy equations of continuous phase. These contributions, referred to as source terms, are calculated using Eq. (j) – (l), given in Table 3. The extent of evaporation of an individual species is based on the saturation concentration of that species in the droplet and in the bulk gas phase; see Eq. (m) in Table 3. The mass evaporated from a droplet in a control volume depends on the time spent by droplet in a cell (t_c), which is decided by the path taken by the droplet in control volume. The path taken by the droplet in control volume is obtained by Eq. (h) and (i). The energy source terms take into account the change in sensible heat of the droplet mass and latent heat associated with the evaporation of species from the droplets. As discussed earlier, 86 wt% of the original feed is evaporated when leaving the mixing nozzle, i.e. at the inlet of the SH1 tubes. All the species evaporate from the droplet simultaneously at their respective evaporation rate based on differences in its vapor pressure and partial pressure. However it is logical to assume that the low boilers start to evaporate earlier than the high boilers. Thus it is assumed that the 86% of the evaporated feed mainly consists of low boilers (i.e. species (a) to (e)) and the remaining 14% of un-evaporated feed mainly consists of high boilers (i.e. species (e) to (k)). The inlet composition of the vapor phase is given in Table 2.

The volume fraction of the droplets at SH1 inlet is about 10^{-3}. Due to complete evaporation of spray droplets a significant (~14%) increase in the continuous phase volume is expected. Thus, the influence of the discrete phase droplets on the turbulence in the continuous phase needs to be considered (Ranade, 2002). For a spray flow rate of 0.077 kg/s with 100 μm diameter droplets the number of droplets entering a mixture superheater tube is about 2×10^8 s^{-1}. Since it is not feasible to simulate such large number of droplets using the Lagrangian approach, a lower but statistically representative number of droplets need to be chosen for the simulations. For this, a sensitivity analysis of the profile of the coke layer that is formed as function of the number of tries per injected droplet is done. Such a sensitivity analysis is also needed when a turbulent dispersion of the droplets is considered. In the present work, the turbulent dispersion of the droplets is also taken into account using the discrete random walk (DRW) model available in FLUENT 13.0. In the DRW model, FLUENT uses the instantaneous velocity ($u=\bar{u}+u'$) in Eq. (h) and (i) in Table 3 to determine the droplet path. The time-averaged fluid velocity ($\bar{u}$) is obtained from the RANS equation (Eq. (c) in Table 1) while the fluctuating component of the velocity (u') is obtained as

$$u'=Rand(0,1)\sqrt{2k/3} \quad (1)$$

In the sensitivity analysis; the simulations are repeated for 1, 5, 10, 20, 30, 40, 50, 60 and 70 tries per droplet injected. It should be pointed out here that there are 315 mesh faces at the inlet of the SH1. Thus, for simulating with 'n_t' no. of tries per droplet trajectory $315\times n_t$ droplets were injected. The magnitude of coke thickness in various zones varied over a large range (10^{-2}–10^{-9} m). Thus, the difference in average coke thickness for entire SH1 tube was similar for various n_t values. In order to amplify the difference in coke thickness profile for each value of 'n_t' the binary cross correlation coefficient was calculated between the coke thickness profile for 'n_t' number of tries and the coke thickness profile obtained with 70 tries per droplet. The binary cross correlation coefficient was calculated using Eq. (2) and is shown in Fig. 3.

$$Correl(\theta_{n_t},\theta_{n_t=70})=\frac{\sum(\theta^Z_{n_t}-\overline{\theta}_{n_t})(\theta^Z_{n_t=70}-\overline{\theta}_{n_t=70})}{\sqrt{\sum(\theta^Z_{n_t}-\overline{\theta}_{n_t})^2\sum(\theta^Z_{n_t=70}-\overline{\theta}_{n_t=70})^2}} \quad (2)$$

It should be noted that the value of this coefficient is above 0.99 for all the cases. It is found that 20 tries per droplet trajectory gave an almost similar result to that obtained for 70 tries. Thus the coke profile obtained from 20 tries per droplet trajectory was found to statistically represent the same result as for a very large number of droplets. Hence all the discrete phase simulations are done with 20 tries per droplet trajectory, i.e. (20 tries × 315 droplets) 6300 droplet being injected normal to the inlet of the SH1. As the droplets move through the mixture superheater tube, they can

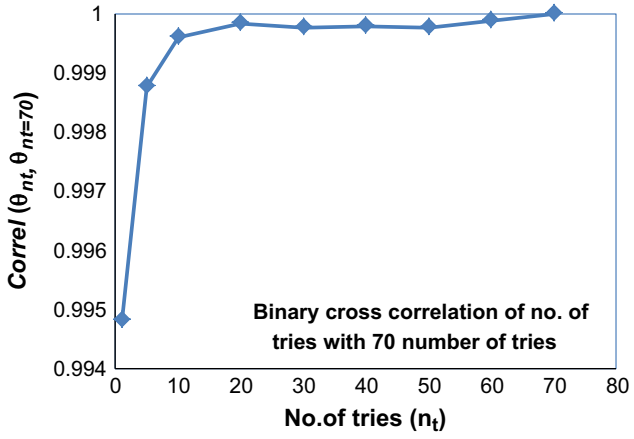

Fig. 3. Cross correlation function for various number of tries per droplet injection in a discrete phase simulation.

splash into a number of smaller droplets. This results in the formation of up to 40,000 droplets which are then tracked while flowing through the mixture superheater tube. The splashed number of droplets will vary for each simulation case based on the operating conditions. The composition of the daughter droplets generated after 'Splash' equals the composition of the impinging droplet. The diameter and the velocity of the daughter droplet are determined based on the droplet–wall interaction model, as discussed in the next section.

3.2. Droplet–wall interaction model

A correct description of the droplet–wall interaction is an essential feature in the spray flow simulations. Because these interactions control the extent of liquid deposited on the superheater tube wall and, hence, the thickness of the coke layer formed on the inner tube wall. When a droplet impinges on the hot superheater tube wall it can rebound from wall, stick the wall or splash into smaller daughter droplets. This depends on momentum of droplet normal to the tube wall (inertia i.e. density and velocity), the adhesive forces between the tube wall and the droplet (viscosity and vapor present between the droplet and the wall) and the energy dissipation due to droplet deformation upon impingement (viscosity, surface tension). The droplet behaviors which will be later extensively used in analyzing the results are described here briefly for clarity.

In 'Stick' the entire mass of the droplets ends up sticking to the wall. This happens when the wall temperature is below the boiling point of the droplet and the inertia of the droplet is not high enough to break the impinging droplet into smaller droplets. However, a little deformation of the droplet or spread over the wall would be possible. Once the liquid comes in physical contact with wall the adhesive forces (between the liquid and the tube wall) and viscous dissipation (droplet deformation on the wall) become dominant and the droplet loses all its momentum. The mass of the impinging droplet is added to the mass of the liquid already deposited on the tube wall.

In 'Rebound' the droplet bounces off the wall, without a significant loss of droplet mass but with a small loss of momentum normal to the wall. 'Rebound' occurs when the tube wall temperature is very high and the momentum (normal to wall) of the droplet is low. At such high wall temperatures, an instantaneous evaporation of the liquid creates a thin vapor film (film boiling) between the droplet and the tube wall. Due to a low momentum (normal to wall) the droplet cannot penetrate in the vapor layer. This restricts the physical contact between droplet and wall, as a result of which the droplet rebounds away from the wall. In 'Rebound' the surface forces are dominant.

In 'Splash', the droplet breaks into multiple smaller daughter droplets upon impinging on the wall. However, a fraction of the impinging droplet mass sticks to the wall. 'Splash' occurs when the momentum (normal to wall) of the droplet is very high. The inertia of the droplet dominates the surface forces, viscous forces and adhesive forces. Upon impingement the droplet first spreads on the wall. The droplet spreading increases the surface area. The surface tension causes ligaments to appear at the outer boundary of the spreading liquid. The ligaments further break into multiple (daughter) droplets. The number, velocity and size of daughter droplets depend on the normal momentum of the droplet at the time of impingement.

The above described post-impingement behavior of a droplet can be predicted by a regime map. The regime map (Fig. 4) essentially categorizes the droplet–wall interaction phenomena based on the wall temperature and physical forces mentioned above i.e. inertial, viscous and surface forces. Fig. 4a presents the regime map of Lee and Ryu (2006) based on the work of Bai and Gosman (1995) for reference. Fig. 4b shows the simplified version of the regime map of Lee and Ryu (2006) used in the present work.

The simplifications were done so as to simulate the droplet–wall interactions which are relevant to the present case. The regime map of Lee and Ryu (2006) distinguishes between 'Boiling induced break-up', 'Break-up', 'Spread' and 'Stick'. In the 'Stick' regime the droplet sticks to the wall at the point of impingement without deformation. In the 'Spread' regime, the droplet spreads over the wall, yet maintaining its singularity. In the 'Break-up' regime the droplet spreads over the wall upon impact to form several daughter droplets. Yet, all the formed droplets remain on the wall. In the 'Boiling induced break-up' the liquid deposited on the wall undergoes break-up due to boiling. In all four regimes mentioned above ('Stick', 'spread', 'break-up' or 'boiling induced break-up') the entire mass of droplets sticks to the wall. In the present study, the four regimes namely 'Stick', 'spread', 'break-up' or 'boiling induced break-up' of the regime map of Lee and Ryu (2006) are considered to be the same as the 'Stick' regime with subsequent evaporation. In contrast to the model of De Schepper et al. (2010), the present model takes into account the evaporation of liquid from the heated wall once the droplet mass sticks to it.

Also, as per the regime map of Lee and Ryu (2006), the 'Rebound' and 'Rebound induced break-up' is said to occur above the Nukiyama temperature (T_{NU}). The Nukiyama temperature (T_{NU}) is the temperature at which the critical heat flux is obtained and the rate of evaporation is also the highest as the liquid droplet is in physical contact with heated wall (Mills and Fry, 1982). Instead it would be logical to assume that that pure 'Rebound' behavior would not occur above T_{NU} but above the Leidenfrost temperature (T_{LF}). T_{LF} is the temperature at which the film boiling begins and at which there is a consistent vapor film between the wall and the droplet. Thus in the present work 'Rebound' and 'Rebound induced breakup' are assumed to occur above T_{LF}. T_{LF} is $\sim$10 K higher than T_{NU} for alkanes (Mills and Fry, 1982).

The regime map of Lee and Ryu (2006) shows a rebound regime below the boiling point (T_B). Whereas, the regime map of Grover and Assanis (2001) shows only stick behavior for wall temperatures below boiling point. As per the co-relations given by Yoon and DesJardin (2006), for wall temperature below boiling point the rebound occurs over a limited range of Weber number (1–10) and only for dry wall. Thus, in the present work rebounce of droplet is not considered for wall temperature below T_{LF}.

Following the above qualitative description and justification of the regime map, the next part presents the criteria to identify the various regimes quantitatively. The Weber number used in the regime map

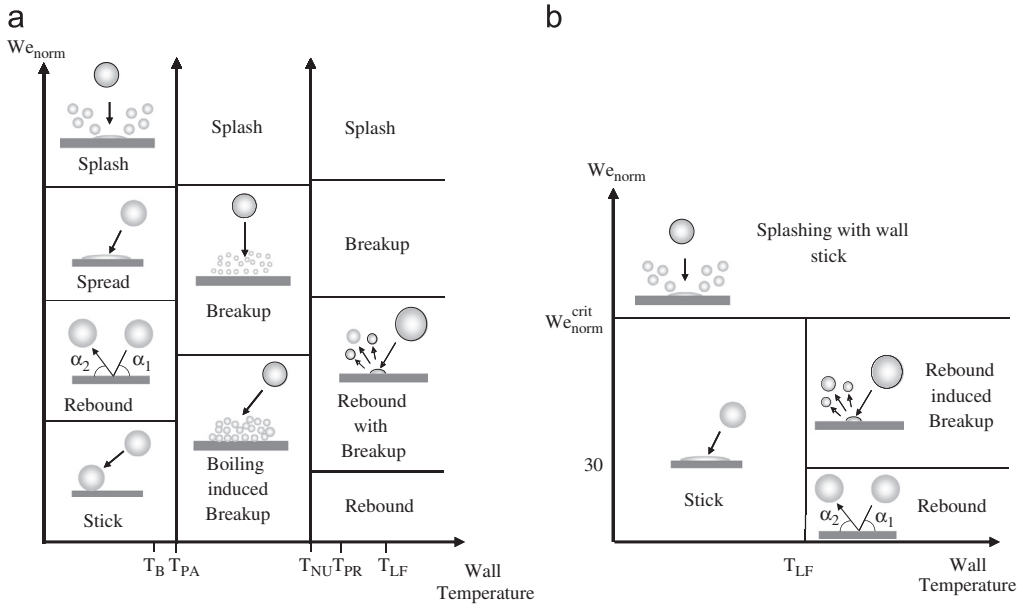

Fig. 4. (a) Regime map of Lee and Ryu (2006) based on work of Bai and Gosman (1995). (b) Regime map as used in presented study for droplet–wall interaction.

and all the subsequent calculations is the normal Weber number of the impinging droplet. It is calculated based on the velocity of the droplet normal to the wall. As mentioned earlier the Leidenfrost temperature is determined by the Leidenfrost effect and indicates the initiation of the film boiling conditions. For alkanes the Leidenfrost temperature is about 52 K above the actual boiling point of the species (Mills and Fry, 1982). It should be mentioned that in the present simulations, as the droplet evaporates, its composition changes (the fraction of high boilers in the droplet will increase) and the Leidenfrost temperature increases correspondingly.

In the present work (Fig. 4b), the 'Stick' regime is observed when the temperature of the tube wall is less than the Leidenfrost temperature ($T_{wall} < T_{LF}$), and the normal Weber number (We_{norm}) is lower than a critical Weber number ($We_{norm} < We^{crit}_{norm}$). The critical Weber number is calculated by Bai et al. (2002) as

$$We^{crit}_{norm} = 1322 \times \left(\frac{\rho\sigma\, d_d}{\mu^2}\right)^{-0.183} \quad (3)$$

Rebound occurs when the normal momentum of the droplet is low ($We_{norm} < 30$) (Wachters and Westerling, 1966) and the tube wall temperature is higher than the Leidenfrost temperature ($T_{wall} > T_{LF}$). Mundo et al. (1995) presented the following empirical expression to relate the normal Weber number of the impinging (We^{I}_{norm}) and the rebounding (We^{R}_{norm}) droplet.

$$We^{R}_{norm} = 0.6785\ \ We^{I}_{norm} \exp(-0.04415\ \ We^{I}_{norm}) \quad (4)$$

Using the above equation the normal velocity of the rebounding droplet can be calculated. The tangential velocity of the rebounding droplet remains unchanged.

For $We_{norm} \sim 80$, Grover and Assanis (2001) present a splashing model in which the impinging droplet splashes into three daughter droplets while some mass of the impinging droplet sticks to the wall. For $We_{norm} \geqslant 80$, Bai et al. (2002) present a model in which the impinging droplet would splash into more than three daughter droplets. The number of daughter droplets formed is function of the normal Weber number of the impinging droplet (We_{norm}) and of the critical Weber number (We^{crit}_{norm}). Thus, the model of Bai et al. (2002) is used to simulate splashing (splashed daughter droplets > 3) and the model of Bai and Gosman (1995) is used to simulate 'Rebound induced breakup' (splashed daughter droplets = 3).

$$\begin{cases} We_{norm} > We^{crit}_{norm} : \text{Splashing} \\ We^{crit}_{norm} > We_{norm} > 30 : \text{Rebound induced breakup} \end{cases}$$

The correlations used to determine the number and the velocity vectors of the daughter droplets and the mass of droplet sticking on the tube wall for the 'Rebound induced breakup' and the 'Splash' regime are presented in Table 4.

3.3. Coking model

Several coke formation mechanisms; including catalytic coke formation and free-radical coke formation have been proposed in literature to describe the coke formation in the reactor tubes of the radiation section of a steam cracker. Catalytic coke formation is observed when the reactants are in contact with a clean metal (steam cracking reactor tubes/coils) or catalyst surface (Albright and Marek, 1988; Froment, 1990). This mechanism of coke formation is seen to occur in the wall temperature range of 1000–1300 K. In the free radical coking mechanism, also referred to as a pyrolytic coking mechanism, the vapor phase species (olefins, aromatics, free radicals) react with the coke layer that has already been formed, e.g. due to catalytic coke formation as described above, on the tube wall. Wauters and Marin (2002) showed that the coke formation rate due to the pyrolytic coking mechanism increases with a factor of 10 for temperature from 1000 to 1100 K. The rate of coke formation was seen to proportional to gas phase radical concentration. The radical concentration was further seen to increase with factor of 10 for every 100 K rise in gas temperatures in the range of 700–900 K. Thus following the above pattern of reduction in rate of coke formation with decrease in temperature the rate of coke formation could be considered to be negligible for the temperature in convection section tube (650–750 K). Coking is also reported to occur downstream the reactor coils, i.e. in the transfer line exchanger (TLE), due to the condensation of the high boilers, either already present in the feed or formed in secondary chemical condensation reactions. As a consequence of lowering the temperature in the TLE, the high boilers form a 'mist'. Upon colliding with the TLE wall the 'mist' sticks to the TLE wall and condenses (Cai et al., 2002). Considering the comparably lower tube wall

Table 4
'Splashing' and 'Rebound induced breakup' models.

Parameter	Splash (Bai et al., 2002)	Rebound induced breakup (Grover and Assanis, 2001)
Number of splashed droplets	$n_S = 5 \times \left(\frac{We_{norm}}{We^{crit}_{norm}} - 1\right)$	$n_S = 3$
Mass of all splashed droplets	$m_S = [0.2 + 0.6\ \ Rand(0,1)]\ \ m_I$	$m_S = m_I = m_1 + m_2 + m_3$
Mean diameter of splashed droplets	$\overline{d_S} = \left(\frac{m_S}{6 m_I n_S}\right)^{1/3} d_I$	
Diameter distribution of splashed droplets	$f(d) = \frac{1}{d_S} \times \exp\left(-\frac{d}{d_S}\right)$	
Energy balance of splashing	$E_{K,S} = E_{K,I} + E_{\sigma,I} - E_D - E_{\sigma,S}$	
Kinetic energy of splashed droplets	$E_{K,S} = \frac{1 m_S}{2 n_S}(V^2_{S,N,1} + V^2_{S,N,2} \ldots V^2_{S,N,nS})$	
Kinetic energy of impinging droplets	$E_{K,I} = \frac{1}{2} m_I V^2_{I,N}$	
Surface energy of impinging droplets	$E_{\sigma,I} = \pi d_I^2 \sigma$	
Surface energy of splashed droplets	$E_{\sigma S} = \pi \sigma \sum_{q=1}^{n_S} d^2_{S,q}$	
Energy dissipated due to liquid deformation on the tube wall	$E_D = \max\left(0.8 E_{KI}, \frac{We_{crit}}{12} \pi d_I^2 \sigma\right)$	$E_D = 0$
Normal velocity of the splashed droplets	$\frac{V_{S,N,q}}{V_{S,N,1}} = \ln\left(\frac{d_q}{d_I}\right) / \ln\left(\frac{d_1}{d_I}\right) \quad (q = 2 \ldots . n_S)$	
Velocity vector of the splashed droplets	$V_{S,q} = 0.95 V_I \times F_T - V_{S,q} \times F_N + 2[0.5 - Rand(0,1)]\ \ F_P$ (Splashing)	
	$V_{S,q} = 0.95 V_I \times F_T - V_{S,q} \times F_N + [0.5 - Rand(0,1)]\ \ F_P$(Rebound induced breakup)	

temperatures of the mixer superheater tubes in the convection section (650–750 K, i.e. boiling range of the gas condensate feed), catalytic coke formation and/or the free radical coking mechanism are very unlikely to occur in superheater tubes.

When over-heated steam is mixed with the partially evaporated liquid feed in the mixing nozzle formation of spray flow is likely. As the spray moves through the mixing nozzle, the low boilers preferentially evaporate from the droplet surface. Thus, the concentration of the high boilers on the droplet surface increases. This increases the resistance against diffusion of the low boilers from the droplet core to the droplet surface. The physical inability of such a droplet to evaporate when it sticks to the tube wall results in thermal degradation and coke formation on the tube wall. Chandrasekharan et al. (2005) developed a steam-feed mixing nozzle to minimize the spray droplets from impinging on the nozzle wall and to reduce the extent of liquid deposition and subsequent coke formation on the nozzle wall. It should be noted that the nozzle is designed to avoid deposition of the droplet on the nozzle wall, but once the droplets enter SH1 tubes, the spray droplets are very likely to impinge on the tube wall, especially near the tube bends, thus resulting in coke formation in the tubes.

It should be noted that not all the liquid mass deposited on the tube wall will get converted into coke. The fraction of the deposited liquid converting into coke depends on the non-volatile fraction of that liquid (at the given wall temperature) and on the asphaltene content of that non-volatile liquid fraction. In order to determine the amount of coke formed from the deposited liquid, the coking model of Wiehe (1993) is used. This model is based on phase separation of the asphaltenes from the liquid. It relies on categorizing the species present in the hydrocarbon feed into four categories, namely volatile species (V), toluene insoluble species (TI), heptane soluble species (H) and heptane insoluble asphaltenes (A). The kinetics of the asphaltene phase separation could be applied to obtain the rate of thermal degradation and corresponding coke formation. Any hydrocarbon feed could be categorized in the above mentioned four species. Thus this model can be applied for any kind of feed to describe thermal degradation.

The following section explains how the asphaltene phase separation mechanism is applied to the present case. Following the hydrocarbon droplets impingement on the tube wall, the volatile species present in the deposited liquid are evaporated into the vapor flow. A species is considered as a volatile species when its vapor pressure at wall temperature is larger than 1/10th of the absolute pressure in the continuous phase. The non-volatile liquid fraction remains on the tube wall. The non-volatile fraction is categorized as toluene insoluble species (TI), heptane soluble species (H) and heptane insoluble asphaltenes (A). The reactant heptane soluble species (H^+) undergo disproportionation and gets converted into product asphaltenes (A^*) and volatiles (V) as per disproportionation-1 (see Table 5). Simultaneously, reactant asphaltenes (A^+) undergo disproportionation to get converted into product heptane soluble species (H^*) and volatiles (V) as per disproportionation-2. A^* are soluble in the heptane soluble species (H^+ and H^*) until their solubility limit (S_L). The excess asphaltenes (A_{ex}) above this solubility limit (S_L) precipitate as a separate hydrogen lean phase in which the asphaltene radical recombination occurs to form toluene insoluble coke (TI) and by product H^*. The above reactions scheme for formation of TI coke results in the following dependency of the amount of insoluble coke:

$$TI = \left(1 - \frac{q}{1 + q \times S_L}\right) \times (a \times H_O - (a + S_L) H_O \times e^{-k_H t} + (m - n \times S_L) A_O \times (1 - e^{-k_A t})) \quad (5)$$

The values for the stoichiometric coefficients (a, m & n), reaction rate constants (k_A and k_H) and solubility of asphaltenes cores (S_L) is obtained experimentally by Wiehe (1993) for the Cold Lake vacuum residue can be found in Table 5.

Based on Eq. (5) the extent of coke formation is presented in Fig. 5. Fig. 5 also presents the extent of coke formation in other feeds containing a varying amount of asphaltenes (A_O) and heptane soluble species (H_O). It is seen that, when the feed is entirely asphaltenic, the coke formation starts immediately and

Table 5
Coking reactions and rate constants (Wiehe, 1993).

Coking reactions	
Disproportionation of heptane soluble species	
$H^+ \rightarrow a \times A^* + (1-a) \times V$	Disproportionation-1
Disproportionation of asphaltenes	
$A^+ \rightarrow m \times A^* + n \times H^* + (1-m-n) \times V$	Disproportionation-2
Conversion of excess asphaltenes to TI coke	
$A_{ex} \rightarrow (1-q) \times TI + q \times H^*$	Disproportionation-3
Excess asphaltene cores	
$A_{ex} = A^* - (S_L \times (H^+ + H^*))$	
Solubility limit (S_L)=0.61(wt/wt)	
Stoichiometric coefficients for above reactions	
a=0.221	m=0.825
n=0.02	q=0.3

also more coke is formed. While, if there are some heptane insoluble species in the feed, an induction period is observed in the coke formation and lesser coke is formed. This induction period corresponds to the reaction time needed for the excess asphaltenes to be formed and the phase separation to be initiated. Depending on the feed composition, the time required to reach the final composition is of the order of 3 to 6 h. The time scale of operation of a steam cracker (radiation section coil decoking) is of the order of 50 days for non-heavy feeds, i.e. ethane and naphtha. Hence, coke formation in the superheater tubes is assumed to be very fast (as compared to the steam cracker operation time scale) and quasi steady state approach is used to simulate the coking kinetics. Thus Eq. (3) is reduced to its steady state form as

$$\mathrm{TI} = \left(1 - \frac{q}{1+q \times S_L}\right) \times (a \times H_O + (m - n \times S_L) A_O) \quad (6)$$

Asphaltenes are the main precursors of coke in the coking model of Wiehe (1993). It should still be pointed out that asphaltenes are not entirely converted into coke, but only the excess asphaltenes precipitate out to form TI coke. The species present in the gas condensate feed used in the present work were all seen to be heptane soluble species. No asphaltenic coke precursors ($A_O=0$) or toluene insoluble species ($TI_O=0$) are present in the feed. Hence, the droplets entering the superheater section contain only heptane insoluble species ($H_O=1$). It should be mentioned here that the present model can be used for any other feed by changing the initial value of asphaltenes (A_O), toluene insoluble (TI_O) and heptane insoluble species (H_O). The coke formation model used by De Schepper et al. (2010) was that of a thermal degradation of fuel in an oxidizing environment. Furthermore, some chemical species were identified as coke precursor species. These pre-cursor species would then be converted into coke as per first order kinetics in the work of De Schepper et al. (2010). Thus higher the temperature, higher was the rate of coke formation. On the contrary, in the present work, as will be seen later, an increase of the wall temperature reduces the extent of coke formed in the tubes. The latter is due to the fact that the extent of non-volatile species residing on the wall reduces with increase in temperature.

4. Solution method

For the studied geometry of the over heater tube, a structured mesh with 1.7 million cells was created. This mesh was selected following a grid sensitivity study as shown in Fig. 6. All the simulations were performed as steady state simulations. First the continuous phase (vapor phase flow) with an inlet flow rate of 1.1 kg/s and an inlet composition as given in Table 2 was

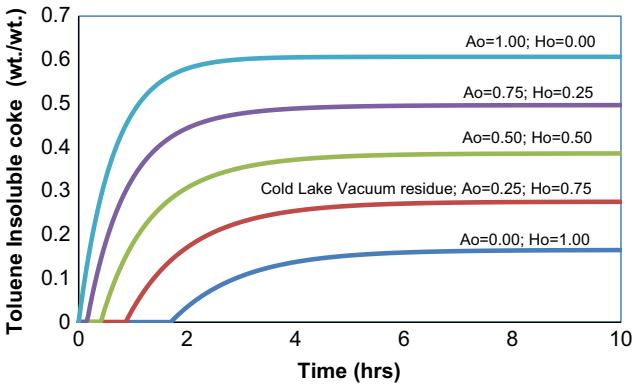

Fig. 5. Toluene insoluble coke formed for varying asphaltene content in the vacuum residue.

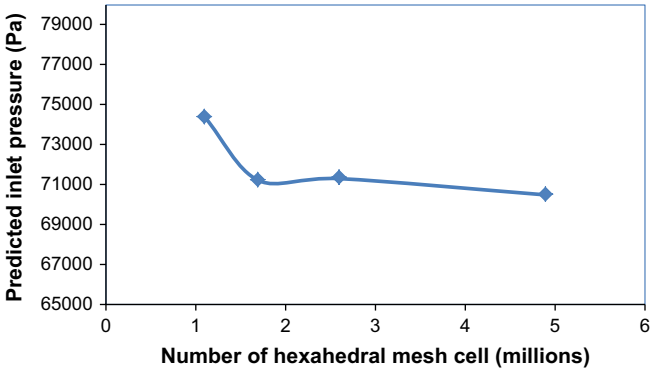

Fig. 6. Mesh dependency of the results.

simulated. Convergence was checked with scaled residuals (a reduction by five orders of magnitude was aimed at) and a mass and heat balance was made (less than 0.01% error between inflow and outflow was requested). Once the continuous phase was converged, discrete phase simulations (spray flow) were started. As two-way turbulence coupling between the continuous and discrete phase was considered. The discrete phase iterations were repeated every 20 continuous phase iterations. The droplet–wall iterations (Stick, Rebound, Rebound induced breakup and splash) as discussed earlier in Section 3.2 was incorporated with user defined functions (UDF). The droplets were injected in the domain normal to the tube inlet using 'surface' injection. The information obtained upon droplet splashing was written in a file during each discrete phase iteration. This information was used to inject the daughter droplets in the subsequent discrete phase iteration using the 'File' type injection approach available in FLUENT. The simulations were considered to be converged once steady state was reached for the species concentrations at the tube outlet. The mass and the composition of the liquid deposited on the wall was then used to determine the amount of volatiles species, non-volatile species and the coke formed on the superheater tube wall.

5. Results and discussion

Fig. 7 presents simulated droplet trajectories for various initial droplet diameters (1, 10, 50 and 100 μm) and for an outer tube wall temperature of 650 K. The spray flow (droplets and evaporated feed) enters normal to the inlet surface of the superheater tube. The inlet is immediately followed by a 90° inlet-bend (Fig. 1). It is clearly observed that the larger droplets (50 and 100 μm) undergo an inertial separation from the vapor flow and impinge on the bend wall opposite to the inlet. All 100 μm droplets are seen to impinge on the tube wall in the inlet-bend, whereas some of the 50 μm droplets enter the horizontal Pass-1 over a short distance before impinging on the Pass-1 wall. For the smaller droplets (1 and 10 μm) very few droplets separate from the vapor flow to impinge on the wall. Since the surface to volume ratio is higher for smaller droplets, the heat and mass transfer rates are also higher. As a result, the smaller droplets are considerably reduced in size due to evaporation in the inlet-bend. Large droplets (100 μm) are subject to evaporation as well, but the corresponding change in droplet diameter is not so significant. The average droplet diameter at the time of impingement in the inlet-bend is 0.47, 7.2, 46 and 96 μm for initial droplet diameters of 1, 10, 50 and 100 μm, respectively. Thus it is seen that 89, 61, 22 and 11% of the initial mass of the droplets is lost by evaporation in the inlet-bend for droplets of 1, 10, 50 and 100 μm initial diameter respectively. Fig. 7 shows that for droplets of 50 and 100 μm initial diameter there is substantial difference in the diameter of droplet before and after

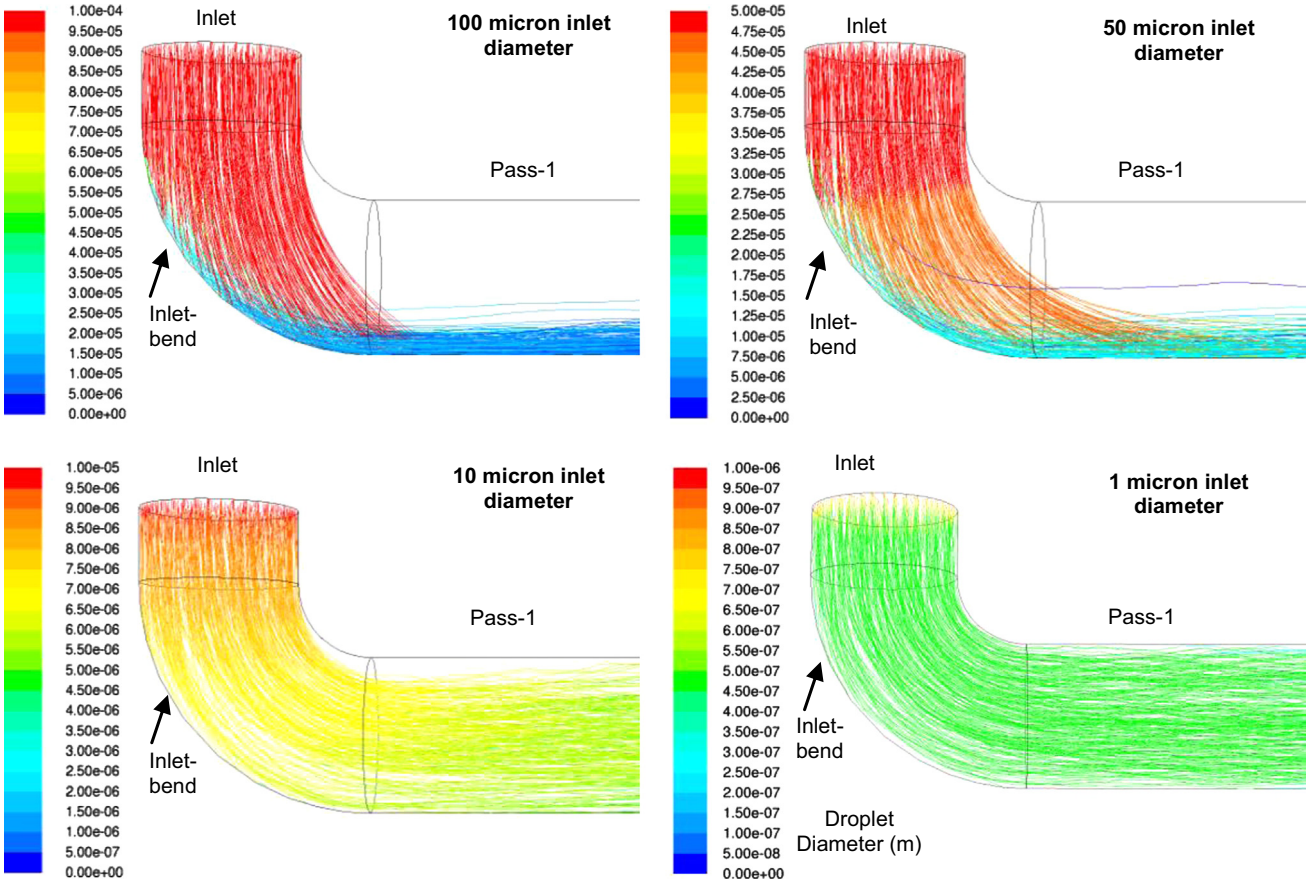

Fig. 7. Droplet trajectories for different droplet diameters.

impingement on wall. This indicates that for larger droplets the reduction in diameter is due to splashing. In all the simulations, the daughter droplets formed due to splashing are further carried along with the main flow into the straight Pass-1 section.

Fig. 8 presents a schematic view of the SH1 tube and the numbered cross-sectional planes (0 to 95) from inlet to outlet. It also presents the average size of droplets crossing these planes for various initial droplet diameters and outer tube wall temperatures. A sudden reduction in the droplet diameter in the first two sections (inlet-bend) is observed. Then, the droplet size gradually reduces till the droplet completely evaporates/sticks to the tube wall. The average droplet size in the cross-sectional plane 1 (exit of the inlet-bend) is 0.47, 6, 21 and 13 μm for initial droplet diameters of 1, 10, 50 and 100 μm respectively. As per the discussion of Fig. 7, the reduction in diameter for smaller droplets (1 and 10 μm) is due to evaporation. While, for larger droplets (50 and 100 μm), the diameter reduction in the inlet-bend is due to splashing. It should also be noted that the droplet diameter in plane-1 for 50 μm of initial droplet size has reduced to 21 μm, while the same for 100 μm initial droplet size the corresponding value is only 13 μm. This is due to the fact that the number and diameter of the daughter droplets generated due to 'Splash' depend on the ratio of the normal Weber number of the impinging droplet and the critical Weber number (Table 4). For a given normal velocity, a 100 μm droplet has a larger normal Weber number than a 50 μm droplet. Thus, a 100 μm droplet produces large number of smaller droplets while a 50 μm droplet generates less but larger droplets upon splashing.

In Pass-1, the change in diameter is seen to proceed at a much slower rate (compared to that in the inlet-bend) and is almost independent of the initial droplet size. This is because; in Pass-1 the reduction in diameter is mostly due to evaporation, which is dependent on the heat available for evaporation (heat transfer rate).

In bend-1 (plane-32) no significant reduction in droplet diameter is observed. However, a significant (40%) reduction in the number of droplets is observed. This shows that the droplets passing through bend-1 undergo 'Stick' rather than 'Splash' (contrary to the inlet-bend). The 'Stick' results from the fact that a small droplet has a normal Weber number lower than the critical Weber number (Eq. (1)). Also the Leidenfrost temperature of the droplet, now mainly comprising of high boilers, is larger than the tube wall temperature. 'Splash' is thus the dominant phenomenon in the inlet-bend while in Pass-1 and bend-1 mostly 'Stick' occurs.

The rate of heat transfer and the evaporative mass loss from the droplets increases with increasing tube wall temperature. For an outer tube wall temperature of 750 K all the droplets are seen to have evaporated before bend-1. On the contrary, for an outer tube wall temperature of 650 K some droplets are seen to even reach the middle section of Pass-2, the second straight tube pass (Fig. 1).

Fig. 9 presents the fraction of incoming liquid that is deposited in the SH1. Liquid is deposited in the tubes when the droplets undergo 'Splash', 'Rebound induced breakup' or 'Stick' upon impingement on the tube wall. As seen from Fig. 9, the highest fraction of liquid is deposited in the inlet-bend due to 'Splash'. For 50 and 100 μm initial droplet diameter a 0.1 fraction of incoming liquid is deposited in the inlet-bend. For 1 and 10 μm initial droplet diameter only a 0.001 fraction of the incoming liquid is deposited in the inlet-bend. Thus for larger diameter droplets the liquid deposition is ~2 orders of magnitude higher than that for smaller diameter droplets. In Pass-1 the average droplet size is

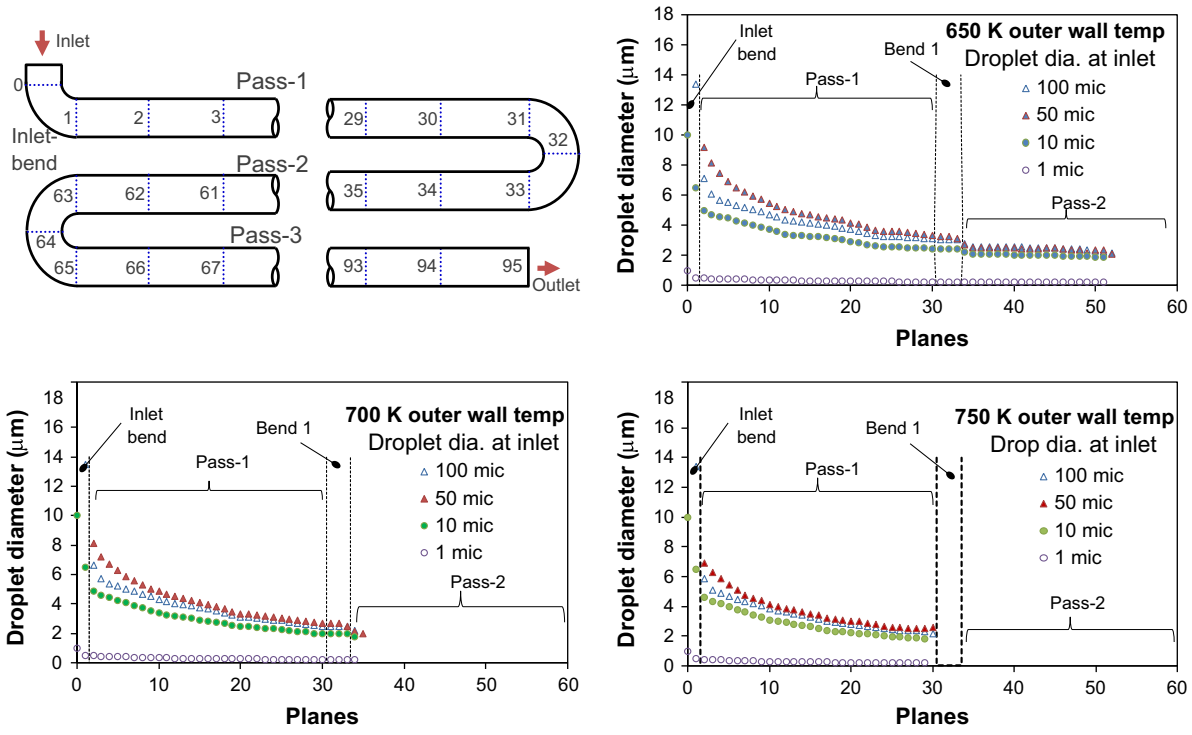

Fig. 8. Average droplet diameter at various locations in the mixer superheater tube for different outer tube wall temperatures.

around 5–10 μm. As a result of which the droplets mostly follow the vapor phase without significant inertial separation. Hence 'Splash' or 'Rebound induced breakup' are rarely observed in Pass-1. The fraction of incoming liquid deposited in Pass-1 is in range of 10^{-7}–10^{-4}. This is almost three orders of magnitude lower than that the deposited fraction in the inlet-bend, where 'Splash' was dominantly observed. As the droplet size further reduces along Pass-1 due to evaporation, the extent of liquid deposition also reduces.

In Fig. 9, it should be noted that although the fraction of incoming liquid deposited in the inlet-bend is higher for larger droplets (50 and 100 μm), but the fraction of incoming liquid deposited in a straight tube pass is higher for smaller droplets (1 and 10 μm). Such a reversal in the liquid deposition trend with droplet diameter is related to the composition of the droplets of different diameter. In the inlet-bend, the droplets with an initial diameter of 50 and 100 μm lose 22 and 11% of their initial mass respectively, due to evaporation. From Table 2 it could be deduced that the droplets at the tube inlet consist of 52% of 'species-e'. Thus even after losing 22% of the initial mass by evaporation a significant amount of 'species-e', with a boiling temperature of 507 K, is found in the droplets. The Leidenfrost temperature of these droplets (~552 K) is lower than the wall temperature (650 K). Initially smaller droplets of 1 and 10 μm diameter loses 89 and 61% of its initial mass by evaporation in the inlet-bend. Thus, the droplets at the exit of the inlet-bend are composed of high boilers only. Thus the Leidenfrost temperature of these droplets is relatively higher (~700 K) than that of the initially larger droplets. As a result of which, for initially smaller droplets more 'Stick' is observed while for initially larger droplets 'Rebound' is observed in Pass-1 for a outer wall temperature of 650 K. Thus, there is a difference in mass deposition on the tube wall for smaller droplet (1 μm) and larger droplets (50 and 100 μm) at the lower tube wall temperature of 650 K. This difference reduces as the outer tube wall temperature increases. At higher outer tube wall temperatures (700 and 750 K) even the initially smaller droplets undergo 'Rebound'.

Fig. 10 presents the thickness of the coke layer formed in the SH1 tube after 30 days of operation. For an outer wall temperature of 650 K the trend of the coke thickness profile is almost similar to the profile of the deposited liquid (Fig. 9). A coke layer thickness of about 0.01 m is observed in the inlet-bend for sprays with larger initial droplet sizes (50 and 100 μm). For initially smaller droplets (1 and 10 μm) the average coke thickness profile is ~0.001 m. The coke thickness in the straight Pass-1 is seen to be at least three orders of magnitude lower than that in inlet-bend. The coke thickness is seen to be one order of magnitude higher for initially smaller droplets (1 and 10 μm) as compared to initially larger droplets (50 and 100 μm). These observations are expected as similar trends were observed in the liquid deposition (Fig. 9).

The coke thickness profile in the inlet-bend is similar for all three outer tube wall temperatures (650, 700 and 750 K). It should be noted that the mass fraction of liquid deposited in the inlet-bend is independent of the outer wall temperature. This is due to the fact that the inlet-bend is insulated and kept out of flue gas chamber resulting into relatively lower wall temperature as compared to that in straight passes. For the straight Pass-1 the amount of heat available for evaporation of the liquid deposited on wall is dependent on the outer tube wall temperature. Thus with an increase in the outer tube wall temperature, the non-volatile fraction of the species deposited on the wall reduces and the extent of coke formed also reduces. Hence the amount of coke formed in Pass-1 is significantly lower than the coke formed in the inlet-bend.

For higher outer tube wall temperatures (750 K) coking is observed only in the inlet-bend and Bend-1, while the 'Pass-1' remains clean (no coke formation). This is due to the fact that the boiling point of the highest boilers in the feed is 740 K (Fig. 2). Hence whatever the composition of the liquid deposited on the tube wall, it is volatile at this wall temperature and evaporates back into the vapor flow.

In the present case the highest coke layer thickness is seen in the inlet-bend. The results of De Schepper et al. (2010) showed that the thickest coke layer of 8×10^{-4} m (0.8 mm) was formed

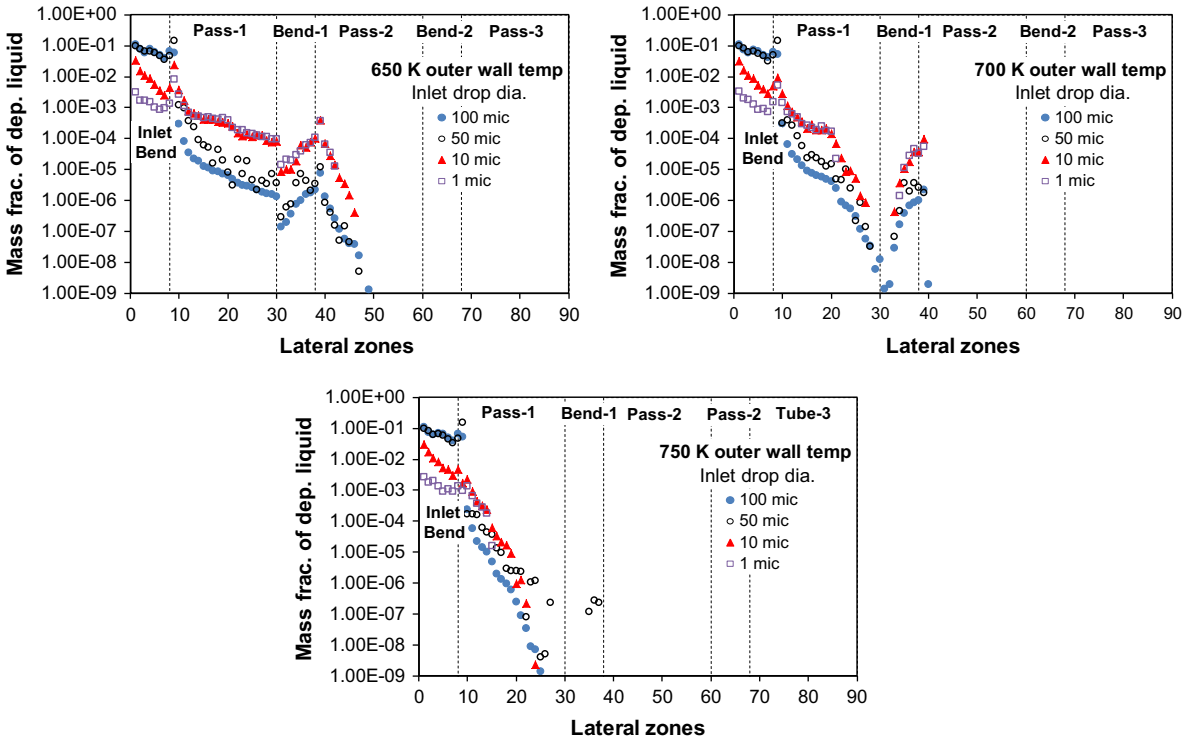

Fig. 9. Mass fraction of incoming liquid deposited on the superheater tube walls.

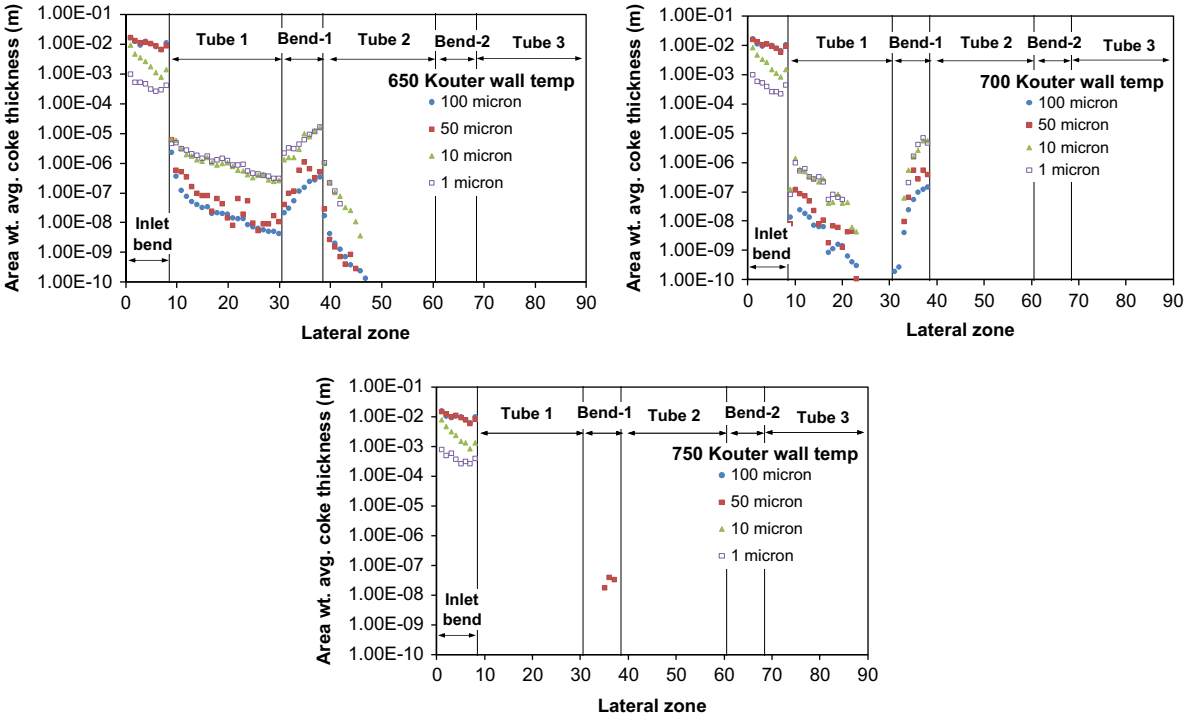

Fig. 10. Coke layer thickness formed in the different tube sections following 30 days of operation.

near the inlet of straight Pass-1. In present study, the thickest coke layer was seen in inlet bend. In present case the coke thickness at the inlet of 'Pass-1' (zones 9) is 10^{-5} m. The difference in the coke thickness in the two studies must be attributed to inclusion of evaporation of liquid deposited on tube wall in present work. The modeling approach of De Schepper et al. (2010) did not consider evaporation of the volatile species in the liquid deposited on the wall. As a result, all the coke precursors present in the liquid deposited on wall was converted into coke. Thus for higher wall temperature the amount of coke formed was also higher. Whereas, the coke model of Wiehe (1993) used in the present work relies on coke formation due to coke precursors present in non-volatile fraction of liquid deposited on the tube walls. The latter approach is more in line with the coke formation mechanism (inability to

completely evaporate the heavy feed) when using a heavy feed in a steam cracker.

6. Conclusions

The coke formation in the superheater tubes of the convection section of a steam cracker is simulated. The spray flow in the superheater is modeled based on an Eulerian–Lagrangian approach using representative species for the gas condensate feed, a multicomponent evaporating droplet model, including droplet–wall interaction to estimate the liquid deposition on the tube wall due to droplet impingement, the removal of volatiles from the deposited liquid, the coke formation from non-volatiles in the deposited liquid and the thermal resistance due to the coke layer formed on the tube wall. The overall results can be summarized as follows

- Incomplete evaporation of the feed in the evaporator and the mixing nozzle generates a spray flow. The spray droplets get deposited on the superheater tube wall. Thermal degradation of deposited liquid results in coke formation.
- The highest mass fraction of incoming droplets is deposited in the inlet-bend of the tube, hence the coke thickness is also highest there.
- Coke formation in the inlet bend could be reduced by reducing the droplet size of the spray flow at the inlet of the superheater.
- The thickness of the coke layer reduces substantially with an increase in the outer tube wall temperature. For wall temperatures above the boiling point of the highest boiling species no coke formation is seen.
- Other possible remedies to avoid coke formation in a superheater are the removal of the high boilers (tail end) from the heavy feed or the upgrading of the heavy feed (e.g. by hydrotreatment).
- The model developed in the present work can be used to evaluate the operational cycle and shutdown frequency for convection section decoking and to select operating parameters to minimize the coke formation in the convection section tubes.

Nomenclature

a	Stoichiometric coefficients for reactions presented in Table 5
A_O	Initial mass fraction of asphaltenes in feed
C_D	Drag coefficient
$C_{P,j}$	Specific heat of species j (J/kg K)
d, d_d	Droplet diameter (m)
d_I	Diameter of impinging droplet (m)
$D_{j,m}$	Species diffusion coefficient in continuous phase (m^2/s)
$d_{S,q}$	Diameter of splashed droplet q (m)
$\overline{d_S}$	Mean diameter of splashed droplets (m)
E	Total energy (J/kg)
$E_{\sigma,I}$	Surface energy of impinging droplet (J)
$E_{\sigma,S}$	Surface energy of splashed droplets (J)
E_D	Energy dissipation during droplet deformation on surface (J)
$E_{K,I}$	Kinetic energy of impinging droplet (J)
$E_{K,S}$	Kinetic energy of splashed droplets (J)
F_N	Unit vector of impinging droplet normal to the surface
F_P	Unit vector perpendicular to F_T and F_N
F_T	Unit vector of impinging droplet tangential to the surface
g	Gravitational acceleration (m/s^2)
G_b	Generation of turbulence kinetic energy due to buoyancy ($kg/m\ s^3$)
G_k	Generation of turbulence kinetic energy due to the mean velocity gradients ($kg/m\ s^3$)
h_{fg}	Heat of evaporation of species j (J/kg)
H_O	Initial mass fraction of heptanes soluble species in feed
I	Unit tensor
J_j	Diffusion flux of species j ($kg/m^2\ s$)
K	Thermal conductivity (J/m K s)
k	Turbulent kinetic energy (m^2/s^2)
k_A	Rate constant for asphaltene disproportionation reaction in Table 5
k_H	Rate constant for heptane soluble species disproportionation reaction in Table 5
k_c	Mass transfer coefficient (m/s)
K_t	Turbulent thermal conductivity (J/m K s)
La	Laplace number ($\rho\sigma d/\mu^2$)
m	Stoichiometric coefficients for reactions presented in Table 5
m_1, m_2 & m_3	Mass of 1st, 2nd & 3rd daughter droplets created in Rebound induced breakup (kg)
m_d	Mass of droplets (kg)
$m_{d,0}$	Initial mass of droplet (kg)
$m_{d,in}$	Mass of droplet at the inlet of control volume (kg)
$m_{d,out}$	Mass of droplet at the outlet of control volume (kg)
m_s	Mass of daughter droplets created in a splash (kg)
$\dot{m}_{d,0}$	Initial mass flow rate of droplet stream (kg/s)
Δm_d	Change in mass of droplet in control volume due to evaporation (kg)
n	Stoichiometric coefficients for reactions presented in Table 5
n_s	Number of daughter droplets created in a splash
n_t	Number of tries per droplets trajectory
P	Pressure (Pa)
P_{sat}	Saturation pressure or vapor pressure (Pa)
q	Stoichiometric coefficients for reactions presented in Table 5
R	Universal gas constant (J/kg/mol)
$Rand(0,1)$	Random number between 0 and 1
S_E	Energy source term in continuous phase due to discrete phase ($J/m^3\ s$)
$S_{F,i}$	Momentum source term in continuous phase due to discrete phase ($kg/m^2\ s^2$)
S_L	Solubility limit for asphaltene in heptane soluble species
S_M	Mass source term in continuous phase due to discrete phase ($kg/m^3\ s$)
$S_{M,j}$	Species mass source term in continuous phase due to discrete phase ($kg/m^3\ s$)
t	Time (s)
t_c	Time spent by droplet in control volume (s)
T	Temperature (K)
T_∞	Temperature of bulk vapor phase (K)
T_d	Temperature of droplet (K)
$T_{d,in}$	Temperature of droplet at inlet of control volume (K)
$T_{d,out}$	Temperature of droplet at outlet of control volume (K)
TI	Toluene insoluble coke
T_{LF}	Leidenfrost temperature (K)
T_{NU}	Nukiyama temperature (K)
T_{ref}	Reference temperature (K)
Δt	Time step size (s)
u	Velocity, instantaneous velocity (m/s)
u'	Fluctuating component of velocity (m/s)
$\vec{u}$	Mean velocity vector
$u_{d,i}$	Velocity of droplet in i direction (m/s)
u_{IT}	Velocity of impinging droplet tangential to the surface (m/s)

u_{SNq}	Velocity of qth splashed droplet normal to the surface (m/s)
V_I	Velocity vector of impinging droplet (m/s)
$V_{I,N}$	Impinging droplet velocity vector normal to the surface (m/s)
$V_{S,i}$	Velocity vector of ith splashed droplet (m/s)
$V_{S,N}$	Splashed droplet velocity vector normal to the surface (m/s)
We_{norm}	Weber number normal to the surface ($d_\mu{}^2\rho/\sigma$)
We_{norm}^{out}	Weber number normal to the surface for outgoing/rebounded droplet
We_{norm}^{in}	Weber number normal to the surface of impinging droplet
We_{norm}^{crit}	Critical Weber number
x_j	Mass fraction of species j in droplet
y_j	Mass fraction of species j in continuous/vapor phase

Symbols

ρ	Density
σ	Liquid surface tension
$\overline{\theta}_{n_t}$	Average coke thickness over entire SH1 tube for 'n_t' number of tries
$\theta_{n_t}^z$	Coke thickness in Zth lateral zone for 'n_t' number of tries
μ	Liquid viscosity
ε	Turbulent dissipation rate
ρ_d	Droplet density
μ_t	Turbulent viscosity

Subscript

K	Kinetic energy
j	jth species
i	Co-ordinate
d	Droplet
S	Splashed droplet
N, norm	Normal to wall
I	Impinging
σ	Surface
b	Buoyancy
o	Initial
in	Inlet
out	Outlet
E	Energy
z	Lateral zone of the SH1 tube

Superscripts

I	Impinging droplet
R	Rebounding droplet
crit	Critical

Acknowledgment

A. Mahulkar and G.J. Heynderickx acknowledge financial support from the Fund for Scientific Research Flanders (FWO) for the coke formation research under project number 3.G.0022.09. The authors are thankful to Prof. Dr. Kevin Van Geem for providing the feed composition. This work was carried out using the Stevin Supercomputer Infrastructure at Ghent University, funded by the Ghent University, the Hercules Foundation and the Flemish Government—department EWI. Authors acknowledge the 'Long Term Structural Methusalem Funding by the Flemish Government".

References

Albright, L.F., Marek, J.C., 1988. Coke formation during pyrolysis—roles of residence time, reactor geometry, and time of operation. Industrial & Engineering Chemistry Research 27, 743–751.
ANSYS, I., 2010. ANSYS FLUENT Theory Guide 13.0. ANSYS, Inc, PA, USA.
Bai, C., Gosman, A.D., 1995. Development of Methodology for Spray Impingement Simulation, International Congress & Exposition, February 27, Detroit, Michigan, United States, p. 75.
Bai, C.X., Rusche, H., Gosman, A.D., 2002. Modeling of gasoline spray impingement. Atomization and Sprays 12, 1–27.
Cai, H.Y., Krzywicki, A., Oballa, M.C., 2002. Coke formation in steam crackers for ethylene production. Chemical Engineering and Processing 41, 199–214.
Chandrasekharan, K., Kloth, A.G.J., Van Westrenen, J., 2005. Apparatus and Process for Vaporizing a Heavy Hydrocarbon Feedstock with Steam Patent, U.S. (Ed.), C07C004/02 ed. Shell Oil Company, United States.
De Schepper, S.C.K., Heynderickx, G.J., Marin, G.B., 2010. Modeling the coke formation in the convection section tubes of a steam cracker. Industrial & Engineering Chemistry Research 49, 5752–5764.
Froment, G.F., 1990. Coke formation in the thermal-cracking of hydrocarbons. Reviews in Chemical Engineering 6, 293–328.
Grondman, A., 1983. Apparatus for Vaporization of a Heavy Hydrocarbon Feedstock with Steam. In: Office, U.S.p. (Ed.), Shell Oil Company, United States.
Grover, O.R., Assanis, D.N., 2001. A spray wall impingement model based upon conservation principles. In: The Fifth International Symposium on Diagnostics and Modeling of Combustion in Internal Combustion Engines (COMODIA 2001), Nagoya, Japan.
Launder, B.E., Spalding, D.B., 1974. The numerical computation of turbulent flows. Computer Methods in Applied Mechanics and Engineering 3, 269.
Lee, S.Y., Ryu, S.U., 2006. Recent progress of spray–wall interaction research. Journal of Mechanical Science and Technology 20, 1101–1117.
Mills, A.A., Fry, J.D., 1982. Rate of evaporation of hydrocarbons from a hot surface: Nukiyama and Leidenfrost temperatures. European Journal of Physics 3, 152.
Mundo, C., Sommerfeld, M., Tropea, C., 1995. Droplet–wall collisions—experimental studies of the deformation and breakup process. International Journal of Multiphase Flow 21, 151–173.
Ranade, V.V., 2002. Computational Flow Modeling for Chemical Reactor Engineering. Academic Press, Cambridge, USA.
Wachters, L.H., Westerling, N.A.J., 1966. The heat transfer from a hot wall to impinging water drops in spheroidal state. Chemical Engineering Science 21, 1047–1056.
Wauters, S., Marin, G.B., 2002. Kinetic modeling of coke formation during steam cracking. Industrial & Engineering Chemistry Research 41, 2379–2391.
Wiehe, I.A., 1993. A phase-separation kinetic-model for coke formation. Industrial & Engineering Chemistry Research 32, 2447–2454.
Yoon, S.S., DesJardin, P.E., 2006. Modelling spray impingement using linear stability theories for droplet shattering. International Journal for Numerical Methods in Fluids 50, 469–489.